Irisin alleviates hepatic steatosis by activating the autophagic SIRT3 pathway

Ying Zhao[1], Jia Li[1], Anran Ma[1], Zhihong Wang[1], Yunzhi Ni[1], Di Wu[1], Yue Zhou[1], Na Zhang[2], Li Zhang[1], Yongsheng Chang[3], Qinghua Wang[1,2]

[1]Department of Endocrinology and Metabolism, Huashan Hospital, Fudan University, Shanghai 200040, China;
[2]Shanghai Innogen Pharmaceutical Co., Ltd., Shanghai 201203, China;
[3]Key Laboratory of Immune Microenvironment and Disease, Department of Physiology and Pathophysiology, Tianjin Medical University, Tianjin 300070, China.

Abstract

Background: Disruption of hepatic lipid homeostasis leads to excessive hepatic triglyceride accumulation and the development of metabolic dysfunction-associated steatotic liver disease (MASLD). Autophagy, a critical process in liver lipid metabolism, is impaired in MASLD pathogenesis. Irisin, a skeletal muscle-driven myokine, regulates lipid metabolism, but its impact on hepatic lipid metabolism is not well understood. Here, we aimed to explore the role of irisin in hepatic steatosis and the underlying mechanisms involved.

Methods: A high-fat diet (HFD)-induced MASLD mouse model was used, and the recombinant irisin protein, herein referred to as "Irisin", was intraperitoneally administered for 4 weeks to evaluate the effects of irisin on hepatic lipid accumulation. Liver tissues were stained with Oil red O (ORO), and triglyceride (TG) and total cholesterol (TC) contents were measured in serum and liver homogenates. The expression of the autophagosome marker microtubule-associated protein 1 light chain 3 (LC3), the autophagy receptor protein sequestosome-1 (SQSTM1/p62), autophagy initiation complex unc-51-like kinase 1 (ULK1) and the lysosomal functional protein cathepsin B was measured via Western blotting, and the expression of the transcription factor EB (TFEB) was analyzed via immunofluorescence to explore autophagic changes. The effect of irisin on autophagic flux was further evaluated in palmitic acid-induced HepG2 cells by measuring autophagic degradation with chloroquine (CQ), and analyzing the colocalization of LC3 and lysosome-associated protein 1 (LAMP1). The possible mechanism was examined by measuring the expression of the autophagic sirtuin 3 (SIRT3) pathway and further validated using overexpression of SIRT3 with plasmid transfection or small interfering RNA (siRNA)-mediated knockdown. Student's *t*-test was utilized for statistical analysis.

Results: Irisin significantly reduces hepatic lipid accumulation in mice fed with HFD, accompanied by enhanced hepatocyte autophagy and upregulation of the SIRT3 pathway. In HepG2 cells, Irisin attenuated palmitic acid-induced lipid accumulation, which was partially dependent on SIRT3 levels. Mechanistically, Irisin treatment upregulated SIRT3 and phosphorylated AMP-activated protein kinase (AMPK), inhibited mammalian target of rapamycin (mTOR) activity, promoted TFEB nucleus translocation, increased cathepsin B expression, enhanced autophagic degradation, and alleviated hepatic steatosis. No significant changes in phosphorylation of ULK1 in the hepatocytes were observed. However, when siRNA was used to knock down *SIRT3*, the changes of those protein were partially reversed, and hepatic steatosis was further exacerbated.

Conclusions: Our findings highlight irisin as a potential therapeutic for hepatic steatosis by modulating autophagy and lipid metabolism, potentially providing a novel therapeutic target for the management of MASLD. Further research is needed to elucidate the underlying mechanisms and explore the potential clinical applications of this approach in the treatment of MASLD.

Keywords: Autophagy; Fatty liver; Irisin; Lipogenesis; Lipid metabolism; Sirtuin 3

Introduction

Metabolic dysfunction-associated steatotic liver disease (MASLD), previously known as non-alcoholic fatty liver disease (NAFLD), is characterized by excessive hepatic triglyceride (TG) accumulation.[1,2] The increasing global prevalence of MASLD is an increasing challenge in metabolic disease populations, posing a significant public health burden. The proportion of MAFLD in an urban Chinese population has reached as high as 28.77%.[3] Despite enormous global efforts, the development of effective therapies based on traditional methods and targets has been largely unsuccessful. More safe and effective treatment strategies are needed.

Access this article online

Quick Response Code:

Website: www.cmj.org

DOI: 10.1097/CM9.0000000000003427

Ying Zhao and Jia Li contributed equally to this work.

Correspondence to: Dr. Qinghua Wang, Department of Endocrinology and Metabolism, Huashan Hospital, Fudan University, Shanghai 200040, China
E-Mail: qh_wang@fudan.edu.cn

Chinese Medical Journal 2026;139(3)
Received: 07-07-2024; **Online:** 18-02-2025 **Edited by:** Yuanyuan Ji

Exercise has beneficial effects on metabolic diseases and can manage the pathologic progression of MASLD.[4–6] Aerobic exercise with moderate-intensity or high-intensity training reduces liver fat and visceral adipose tissue without clinically significant weight loss.[7–9] The mechanism of fat loss independent of weight loss is unknown. During exercise, skeletal muscle releases various myokines, which benefit metabolic homeostasis.[10]

Irisin is an exercise-induced myokine that is proteolytically cleaved from the N-terminus of fibronectin domain III containing 5 (FNDC5) and secreted into the circulation, where it potentially functions in systemic metabolism.[11,12] Some studies have suggested that serum irisin concentrations are associated with hepatic lipid contents in obese or fatty liver patients.[13,14] However, a meta-analytical review revealed that circulating irisin levels in NAFLD patients did not differ from that in non-NAFLD controls and were independent of disease severity or racial differences.[15]

Research has indicated that irisin increases the oxidation of fatty acids and reduces fat weight in diabetic mice.[16,17] Irisin has the potential to inhibit inflammation and ameliorate lipid metabolic derangements.[18–21] These findings suggest that irisin may mediate the beneficial effects on hepatic lipid metabolism. Despite the extensive documentation of the influence of irisin on these factors, its precise role in regulating hepatic lipid metabolism and its implications for the development of MASLD remains to be elucidated. Developing protein drugs that align with irisin characteristics remains a challenge. In this study, we developed an irisin-IgG Fc fusion protein through the genetic engineering of recombinant fusion proteins.[22,23] This long-acting modification has the potential to overcome the short half-life limitation of native irisin, thereby enhancing its clinical applicability.[24]

Autophagy plays a critical role in maintaining the homeostasis of cellular materials.[25] The process of autophagy that is involved in the lipolysis of lipid droplets is referred to as "lipophagy," which plays a key role in inhibiting lipid droplet accumulation.[26,27] Impaired autophagy has been linked to the pathogenesis and development of MASLD.[28,29] The downregulation of autophagy genes and increased lipid accumulation in *FNDC5*$^{-/-}$ mouse livers provide further evidence that regulation of autophagy may constitute an important therapeutic mechanism in the treatment of MASLD.[30]

In this study, we investigated if irisin fusion protein has the potential to mitigate hepatic steatosis by increasing autophagic flux, which subsequently promotes hepatic lipid degradation.

Methods

Materials

Recombinant irisin protein, herein referred to as "Irisin", was obtained from Yinnuo Pharmaceutical Technology Co., Ltd (Shanghai, China). The production involved a platform technique previously described elsewhere.[22,23] The C-terminus of irisin was fused with an IgG Fc fragment, designed to extend its *in vivo* half-life and facilitate detection under both *in vivo* and *in vitro* conditions.

Animal experiments and experimental design

To study the therapeutic effect of Irisin on hepatic steatosis, six-week-old male C57BL/6J mice were randomly divided into two groups. A normal chow diet (NCD, n = 6) with 11.3% kcal fat, 63.6% kcal carbohydrate, and 25.1% kcal protein (1010112, Jiangsu Xietong, China) was fed to one group, and a high-fat diet (HFD, n = 12) with 60% kcal fat, 20% kcal protein, and 20% kcal carbohydrate (BioServ F3282, Frenchtown, New Jersey, USA) was given to the other for 12 weeks. After 12 weeks, half of the HFD-fed mice were treated with Irisin for the following 4 weeks. The mice in the NCD and HFD groups were administered equal volumes of physiological saline, whereas those in the Irisin-treated group were injected with an intraperitoneal injection of 1.5 mg/kg of Irisin twice a week. Body weights were monitored weekly in each group until the mice were anesthetized for further analysis. All animals were bred and housed at a constant temperature of 22°C–24°C, 50–60% humidity, and a 12/12-h light/dark cycle with free access to food and water. Animal care procedures were approved by the Animal Care and Use Committee of the Fudan University Shanghai Medical College and followed the National Institute of Health guidelines (No. 2023-HSYY-566JZS) on the care and use of animals.

Cell culture and hepatic steatosis model induction

The human hepatocellular carcinoma HepG2 cell line was acquired from the Type Culture Collection of the Chinese Academy of Sciences (Shanghai, China). Then, the cells were cultured in high-glucose Dulbecco's modified Eagle medium containing 10% foetal bovine serum, 10 μg/mL streptomycin, and 100 μg/mL penicillin. The cells were exposed to 300 μmol/L palmitic acid (PA, P9767, Sigma-Aldrich, Germany) for 24 h to establish a model of cellular hepatic steatosis and were cocultured with different doses of Irisin (0–100 nmol/L) to detect various indicators after 24 h.

Determination of the half-life of the Irisin

Fasting blood was obtained carefully from the mouse orbital venous plexus (n = 4), followed by a single injection of Irisin (i.p., 1.5 mg/kg). The samples were collected for 6 consecutive days and centrifuged at 1000 ×g for 30 min at 4°C. The drug concentrations were detected using the Irisin detection kit (EQ027943HU, Huamei Technology Co., Ltd., Wuhan, China). The recombinant fusion proteins (Irisin) resulted in enhanced structural stability, which led to an extended *in vivo* half-life ($t_{1/2}$ = 76 h in mice) and a profound pharmacokinetic profile with enhanced efficacy in animal models. Pilot studies suggested an *in vivo* treatment regime involving two weekly injections [Supplementary Figure 1, http://links.lww.com/CM9/C262].

Determination of autophagic flux

The cells were pretreated with 50 μmol/L chloroquine (CQ) (C6628, Sigma Aldrich, Germany), an autophagosome degradation inhibitor,[31] for 4 h before palmitic acid and Irisin treatment. The autophagic flux index was evaluated as described previously: autophagy flux index = (light chain 3 [LC3]-II expression levels with CQ)/(LC3-II expression levels without CQ).[32] The LC3-II expression level was normalized to that of glyceraldehyde-3-phosphate dehydrogenase (GAPDH). The autophagic flux index of the control group was set as 1 in each experiment.

Western blotting

The samples of HepG2 cells and liver tissue were lysed via radio-immunoprecipitation assay (RIPA) buffer, and the protein concentrations were measured. Then, 10–20 μg protein samples were loaded and separated via sodium dodecyl-sulfate polyacrylamide gel electrophoresis (SDS–PAGE) and subsequently transferred to polyvinylidene fluoride (PVDF) membranes. Five percent milk was used to block the membranes for one hour at room temperature. The membranes were subsequently incubated with primary antibodies against LC3 (ab192890, Abcam, UK), p62 (ab109012, Abcam), cathepsin B (31718, Cell Signaling Technology, USA), lysosome-associated protein 1 (LAMP1; 15665, Cell Signaling Technology), sirtuin 3 (SIRT3; ab217319, Abcam), p-AMPK (50081, Cell Signaling Technology), AMPK (5832, Cell Signaling Technology), p-mTOR (2974, Cell Signaling Technology), and mTOR (2983, Cell Signaling Technology) at 4°C overnight, following the manufacturer's instructions. The blots were then exposed to the relevant secondary antibodies for an hour, after which chemiluminescence was used to visualize the proteins. GAPDH served as the internal standard. Each experiment was repeated at least three times, and densitometric analysis of the Western blotting signals was performed via ImageJ software (National Institutes of Health, Bethesda, MD, USA).

Biochemistry

Blood samples collected from the mouse orbital venous plexus were placed into a centrifuge at 1000 ×*g* for 30 min to obtain the serum. Liver tissues were mixed with anhydrous ethanol at a ratio of 1:9 and then thoroughly centrifuged at 2500 ×*g* in an environment of 4°C for 10 min to obtain the supernatant for biochemical research. Relevant assay kits (A110-1, A111-1, C009-2-1, and C010-2-1, Nanjing Jiancheng Bioengineering Institute, China) were used in strict accordance with the instructions to determine the biochemical indicators in the serology and liver homogenates.

Immunocytochemistry and immunohistochemistry

The hepatic samples were fully processed after fixation with 4% paraformaldehyde and incubated with primary antibodies against LC3, p62, cathepsin B, and transcription factor EB (TFEB; 13372-1, Proteintech, USA) at 4°C. After 24 h, the samples were incubated with secondary antibodies for 1 h at room temperature. Then, the cells were treated with 4′,6-iamidino-2-phenylindole dihydrochloride (DAPI) solution in the dark for 5 min. Images were captured via a fluorescence microscope, and five images were randomly taken for each sample. Image-Pro Plus version 6.0 (Media Cybernetics, Bethesda, MD, USA) was used to analyze the fluorescence intensity.

Oil red O (ORO) staining

The lipid content of cells or tissues was semiquantified via using ORO staining. HepG2 cells or liver slices were immersed in 60% isopropanol after fixation with 4% paraformaldehyde. The samples were subsequently stained with a freshly prepared ORO dye solution (O0625, Sigma-Aldrich, Germany) for 30 min (oil red: deionized water = 3:2), followed by incubation with hematoxylin for 1 min. The results were observed under an optical microscope after thorough washing with phosphate buffered saline (PBS) and distilled water. Images obtained from the ORO-stained sections were calibrated via Image-Pro Plus 6.0 software, and a threshold was set on the basis of the relative range of staining intensity. All the images were obtained at a consistent threshold, and a percentage threshold area was calculated for each image. Five random images were obtained for each sample, and the relative staining intensity for each sample was calculated by averaging the area percentages.

Hematoxylin and eosin (HE) staining

Livers were fixed in 4% paraformaldehyde at 4°C overnight. The fixed tissues were subsequently dehydrated in a gradient of ethanol, hyalinized in xylene, embedded in paraffin wax, and sectioned at a thickness of 5 μm. An HE staining kit (ScyTek Laboratories, West Logan, USA) was used for the pathological evaluation of the livers. Photographs were captured using a Leica DMI3000 microscope (Leica Microsystems, Germany).

Intraperitoneal glucose tolerance test and intraperitoneal insulin tolerance test

The mice were injected with a 2 g/kg glucose load after 12 h of fasting, and blood glucose levels were measured at 0, 15, 30, 60, 90, and 120 min to assess glucose tolerance (intraperitoneal glucose tolerance test [IPGTT]). The mice were intraperitoneally injected with 0.75 U/kg insulin (Novo Nordisk, Denmark) after 6 h of fasting. Blood glucose levels were measured at 0, 15, 30, 60, 90, and 120 min after insulin administration to assess insulin sensitivity (intraperitoneal insulin tolerance test [IPITT]). All blood samples were collected from the tail veins of mice, and blood glucose levels were measured immediately via a glucometer (Bayer, Germany).

SIRT3 overexpression and knockdown

Plasmid-based *SIRT3* overexpression was procured from Shanghai Genechem Co., Ltd, China. *SIRT3* expression was knocked down in HepG2 cells using small interfering RNA (siRNA) oligonucleotides (Biotend Biotechnology

Co., Ltd., Shanghai, China). Using Lipofectamine 3000 (Invitrogen, USA), the plasmids were transiently transfected into HepG2 cells in strict accordance with the product guide. In brief, HepG2 cells were initially seeded in 24-well plates overnight. The cells were subsequently transfected with 0.5 μg of plasmid or 50 nmol/L SIRT3-siRNA for 24 h. Then, the cells were subjected to treatment with palmitic acid and Irisin. Alterations in autophagy levels and lipid deposition were examined. All the experiments were conducted independently and were repeated three times.

Statistical analysis

All the statistical analyses were performed via GraphPad Prism ver. 6.0 software (GraphPad Software, Inc., San Diego, CA, USA), and the results are presented as the mean ± standard deviation (SD). Student's *t*-test was utilized to examine the differences between the two groups. P <0.05 was considered statistically significant.

Results

Irisin reduces hepatic lipid accumulation

To assess the effects of Irisin on hepatic steatosis, we conducted a comprehensive evaluation of morphological changes and liver weight. HFD-fed mice presented significant hepatomegaly and visibly yellowish discoloration of the liver, indicative of steatosis. In contrast, the livers of the mice treated with Irisin appeared nearly normal in size and displayed a healthier reddish color [Figure 1A]. The results of the quantitative analysis revealed that the liver weight of the HFD-fed mice was 2.3-fold greater (t = 8.8, P <0.05) than that of the NCD-fed mice, which was mitigated by 15.7% upon Irisin treatment (t = 5.1, P <0.05). The weights of epididymal white adipose tissue (eWAT) and inguinal white adipose tissue (iWAT) were significantly greater in HFD-fed mice than in NCD-fed mice, and were lower after Irisin treatment (t = 4.6, P <0.05; t = 3.9, P <0.05) [Figure 1B]. Further study of liver sections from the HFD group revealed pronounced fat droplet accumulation (t = 15.4, P <0.05) within hepatocytes, which was markedly reduced (t = 4.0, P <0.05) in the livers of Irisin-treated mice [Figure 1C]. HE staining of liver tissues revealed a greater ballooning degeneration in the HFD group compared with the NCD group, which was significantly reduced after Irisin treatment [Figure 1D]. Biochemical analysis of liver homogenates from the HFD group revealed remarkable 3.0- and 3.4-fold increases in TG (t = 14.1, P <0.05) and total cholesterol (TC) levels (t = 13.9, P <0.05), respectively, compared with those in the NCD group. Notably, Irisin treatment led to a 13.8% reduction in TG levels (t = 2.3, P <0.05) and a 14.4% reduction in TC levels (t = 2.7, P <0.05) in the liver [Figure 1E]. Similarly, the serum TG and TC levels in the HFD group were significantly elevated by 2.2- and 1.9-fold, respectively, compared with those in the NCD group. However, Irisin administration resulted in a 12.3% reduction in serum TG levels (t = 3.1, P <0.05) and a 17.3% reduction (t = 3.3, P <0.05) in TC levels [Figure 1F]. The serum low-density lipoprotein cholesterol (LDL) levels in the HFD group were greater (t = 15.5, P <0.05) than that in the NCD group. However, these parameters decreased significantly in Irisin treatment groups (t = 2.3, P <0.05). There was no significant difference in food intake and serum high-density lipoprotein cholesterol (HDL-C) levels in the mice in each group [Supplementary Figure 2A and 2B, http://links.lww.com/CM9/C262]. Given the importance of hepatitis, we also measured serum alanine aminotransferase (ALT) and aspartate transaminase (AST) levels in the mice in each group.[33,34] The results demonstrated that ALT (t = 23.2, P <0.05) and AST levels (t = 14.3, P <0.05) were significantly increased in high fat-fed mice. The changes were reduced after Irisin treatment (t = 2.2, P <0.05; t = 2.5, P <0.05) [Supplementary Figure 2C, http://links.lww.com/CM9/C262]. IPGTTs and IPITTs were conducted in mice treated with the Irisin. Our findings demonstrated that glucose tolerance and insulin sensitivity were significantly greater in Irisin-treated mice than those fed with HFD [Figure 1G]. Over a 16-week period of high-fat feeding, the body weights of the mice increased significantly. However, upon treatment with Irisin fusion protein, there was a notable trend toward reduced body weight (t = 2.0, P >0.05) [Figure 1H]. Additionally, we performed an *in vitro* study to determine the appropriate concentration of Irisin for subsequent mechanistic research. The results from ORO staining demonstrated that Irisin dose-dependently reduced palmitate-induced lipid accumulation in HepG2 cells, with a significant difference (t = 4.1, P <0.05) noted at a concentration of 100 nmol/L [Supplementary Figure 3, http://links.lww.com/CM9/C262]. Therefore, we selected this concentration for further *in vitro* mechanistic research on the basis of these findings.

Irisin reduces hepatic lipid accumulation while enhancing autophagy

Impaired autophagy is a hallmark of MASLD models in rodents, including the classic HFD-induced model. Our studies revealed that autophagic flux in hepatocytes is inhibited by reduced cargo degradation in an HFD environment. This results in the inhibition of autophagic flux in hepatocytes, manifested by the accumulation of the autophagosome marker protein LC3-II and the autophagy receptor protein p62. We assessed the effect of irisin on autophagic flux using three methods.

First, Western blotting revealed increases in LC3 (t = 5.5, P <0.05) and p62 (t = 6.5, P <0.05) expression levels in the livers of HFD-treated mice (2.0- and 1.7-fold at the protein level, respectively, relative to their levels in NCD-fed mice). However, these levels decreased by 30% (t = 3.0, P <0.05) and 22% (t = 3.4, P <0.05), respectively, after treatment with Irisin [Figure 2A]. Compared with those in the NCD group, the livers in the HFD group presented 1.5- and 2.0-fold increases in the number of LC3 (t = 9.5, P <0.05) and p62 (t = 13.0, P <0.05) puncta, respectively, according to immunofluorescence intensity analysis. These values decreased by 19.7% (t = 4.6, P <0.05) and 21.5% (t = 4.7, P <0.05) in the Irisin-treated group [Figure 2B, C]. Similarly, Western blotting revealed that, compared with palmitic acid treatment, Irisin treatment

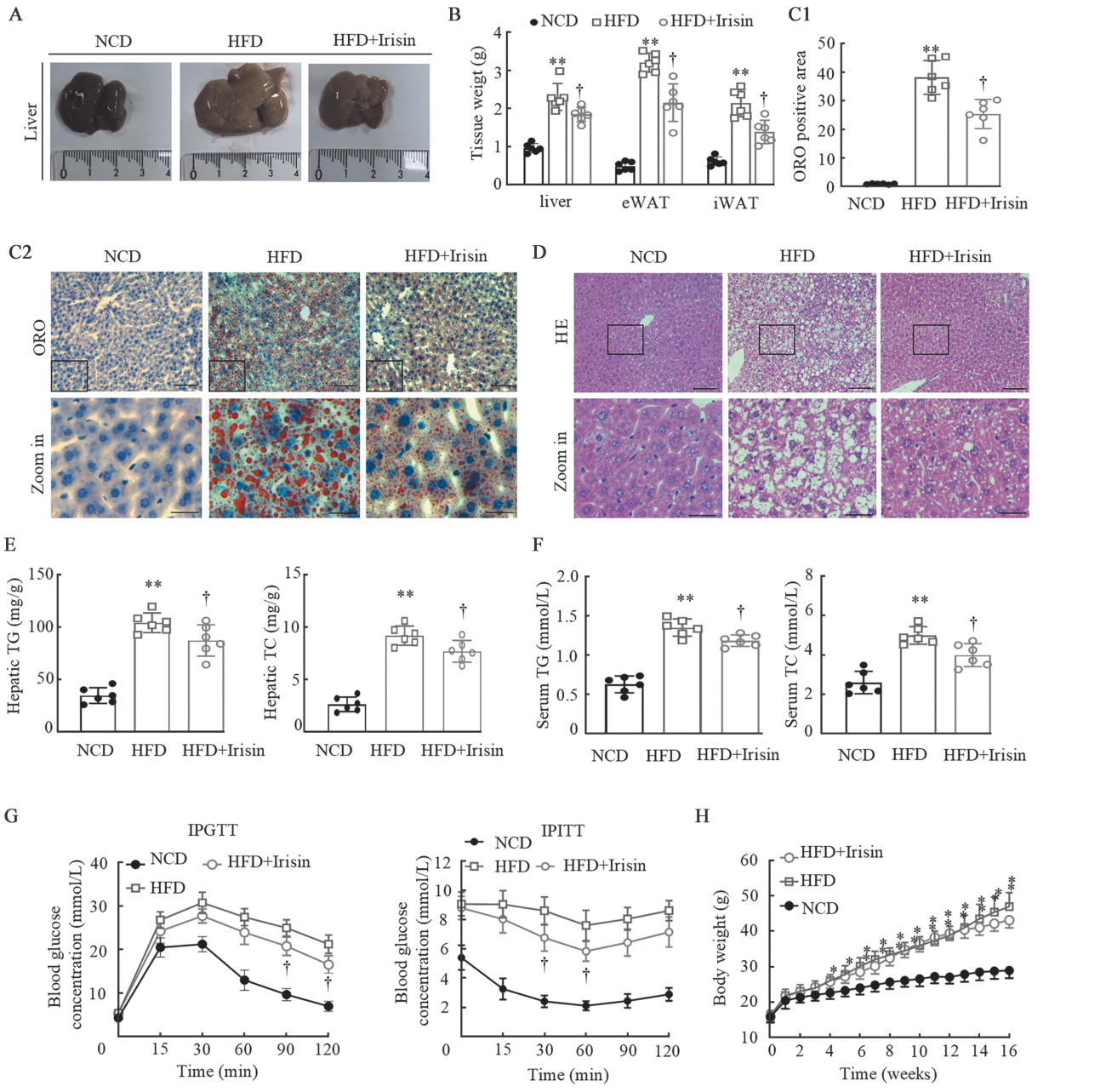

Figure 1: Irisin reduces HFD-induced hepatic lipid accumulation in mice. The mice were fed with HFD for 12 weeks and then treated with physiological saline solution or Irisin for the following 4 weeks. Mice fed an NCD served as controls. All the mice were sacrificed after 16 weeks. (A) Representative images of mouse liver specimens at 16 weeks. (B) Tissue weights of the liver, iWAT, and eWAT. (C1 and C2) ORO staining of the liver and corresponding statistics. The scale bar is = 50 μm in the low-resolution image and 15 μm in the high-resolution image. (D) H&E staining of histopathological liver sections. (E) Changes in triglycerides and cholesterol levels in liver homogenate. (F) Serological indices of TG and TC levels. (G) IPGTT and IPITT. (H) Body weight. The values in the histograms are the mean ± SD from six mice per group. $^{*}P<0.05$, $^{**}P<0.01$ *vs.* NCD, $^{\dagger}P<0.05$ *vs.* HFD. eWAT: Epididymal white adipose tissue; HE: Hematoxylin-eosin; HFD: High-fat diet; IPGTT: Intraperitoneal glucose tolerance test; IPITT: Intraperitoneal insulin tolerance test; iWAT: Inguinal white adipose tissue; NCD: Normal chow diet; ORO: Oil red O; SD: Standard deviation; TC: Cholesterol; TG: Triglyceride.

reduced LC3 ($t = 3.8$, $P < 0.05$) and p62 ($t = 5.1$, $P < 0.05$) expression levels in HepG2 cells. The results of the immunofluorescence intensity analysis of LC3 ($t = 7.1$, $P < 0.05$) and p62 ($t = 4.1$, $P < 0.05$) were consistent with the results of the Western blotting analysis [Figure 3A–C]. Irisin dose-dependently reduced palmitate-induced LC3 and p62 accumulation in HepG2 cells.

Second, we used the autophagic degradation inhibitor CQ to assess the level of autophagic flux. Western blotting revealed that LC3II expression levels were minimally increased ($t = 100.3$, $P < 0.05$) in the palmitic acid group after CQ treatment, compared with those in the palmitic acid group. However, these parameters were significantly greater in the Irisin group with CQ treatment ($t = 4.6$, $P < 0.05$) [Figure 3D]. The fluorescence intensity of LC3 and the Western blotting data were consistent ($t = 2.6$, $P < 0.05$) [Figure 3E].

Third, we labeled autophagosomes (green fluorescence) with LC3 and lysosomes (red fluorescence) with LAMP1 in HepG2 cells. Yellow dots (the overlay of green and

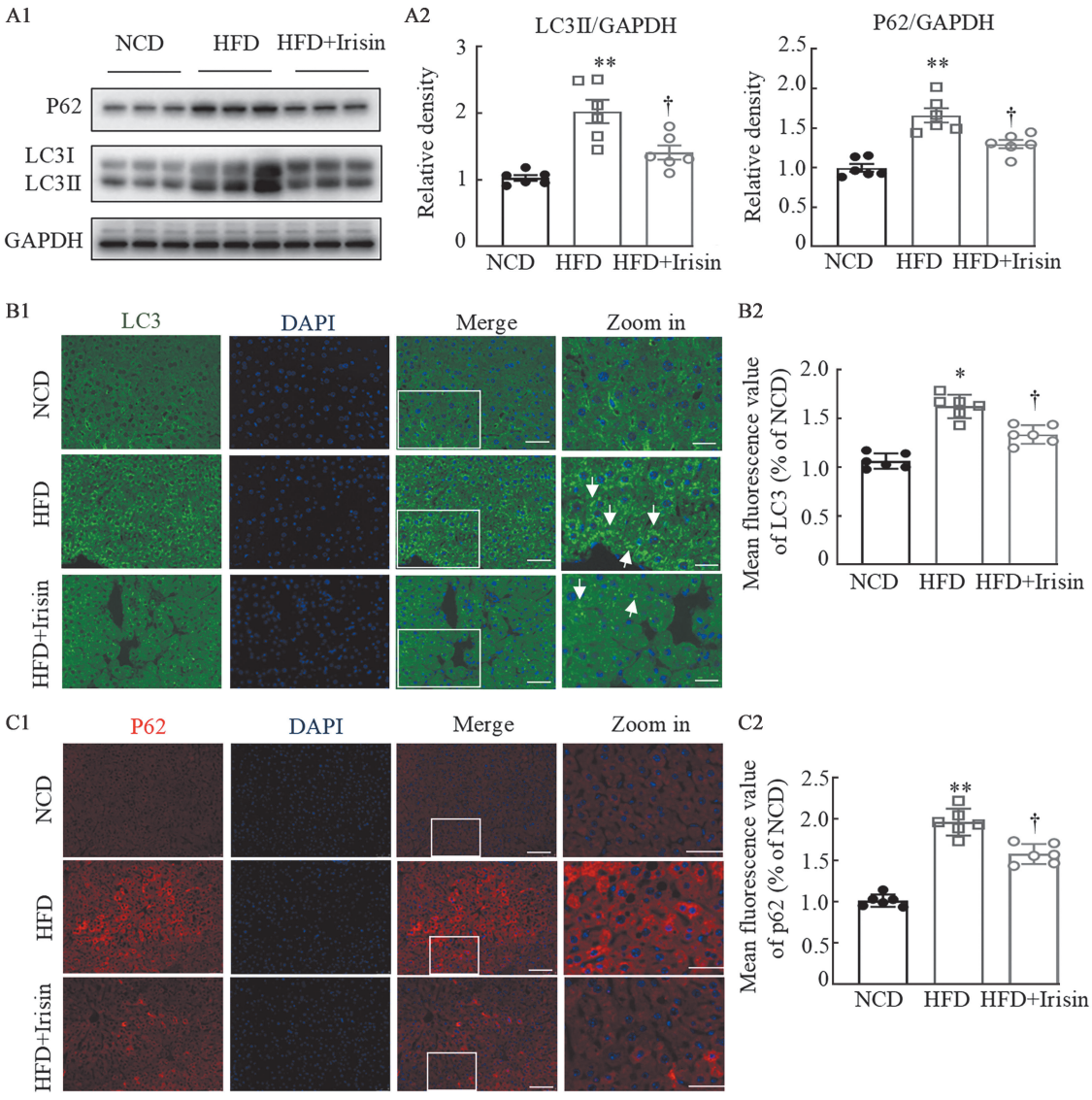

Figure 2: Irisin enhances the degradative capacity of hepatocyte autophagy in HFD-treated mice. (A1 and A2) LC3II and p62 expression levels in the livers of mice from the normal diet, HFD, and Irisin groups at 16 weeks were analyzed by western blotting and statistical analysis. (B1 and B2) LC3 expression levels in the livers of mice from the normal diet, HFD, and Irisin groups at 16 weeks were analyzed by immunofluorescence staining and statistical analysis. The arrows represent the expression levels of LC3 in the livers of mice in different groups. (C1 and C2) P62 expression levels in the livers of mice from the normal diet, HFD, and Irisin groups at 16 weeks were analyzed by immunofluorescence staining and statistical analysis. The scale bars represent 50 μm in the low-resolution image and 25 μm in the high-resolution image. The values in the histograms are the mean ± SD from 6 mice per group. $^{*}P$ <0.05, $^{**}P$ <0.01 *vs.* NCD, $^{\dagger}P$ <0.05 *vs.* HFD. DAPI: 4′,6-iamidino-2-phenylindole dihydrochloride; GAPDH: Glyceraldehyde-3-phosphate dehydrogenase; HFD: High-fat diet; LC3: Light chain 3; NCD: Normal chow diet; SD: Standard deviation.

red fluorescence) indicate labeled autolysosomes. We observed that irisin increased (t = 6.9, P <0.05) the number of autolysosomes in the merged image via confocal microscopy [Figure 3F]. Moreover, we detected minimal changes in the fluorescence intensity of the endo-lysosomal marker LAMP1 in both the palmitic acid treatment group and the Irisin treatment group. Collectively, these results demonstrate that irisin promotes autophagosome degradation and enhances autophagic flux.

Irisin enhances autophagy in hepatocytes independent of phagophore formation

We evaluated the phosphorylation level of unc-51-like kinase 1 (ULK1), a critical regulator of phagophore formation.[35] Our results revealed that irisin did not significantly affect the expression of p-ULK1 in the liver (t = 0.7, P >0.05) of HFD-treated mice [Supplementary Figure 4A, http://links.lww.com/CM9/C262] or palmitate-treated HepG2 cells (t = 0.7, P >0.05) [Supplementary Figure 4B, http://links.lww.com/CM9/C262]. These results imply that irisin does not influence the formation of phagophores in the liver.

Irisin enhances autophagy in hepatocytes, and is associated with improved lysosomal function

Lysosomes play a pivotal role in autophagy-induced lipid droplet degradation.[36] Therefore, we investigated the impact of irisin on lysosomal function. Cathepsin B,

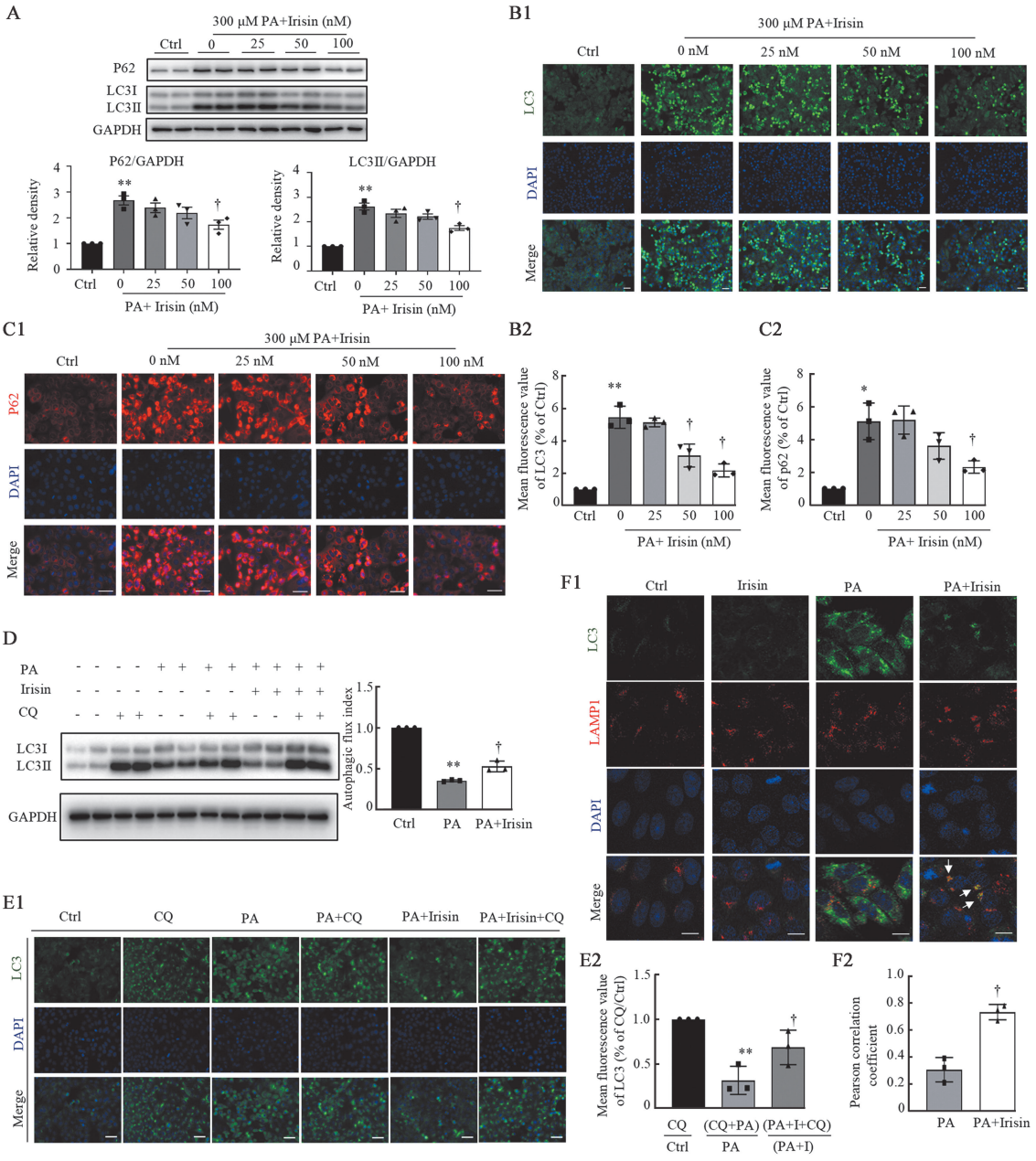

Figure 3: Irisin increases autophagic flux in HepG2 cells treated with palmitate. (A) HepG2 cells were treated with control DMEM or 300 μmol/L palmitate and incubated with different doses of Irisin (0–100 nmol/L) for 24 h. LC3II and p62 expression levels were analyzed by Western blotting and statistical analysis in HepG2 cells. (B1 and B2) LC3 expression levels are analyzed by IF staining and statistical analysis in HepG2 cells. Scale bar: 50 μm. (C1 and C2) P62 expression levels are analyzed by IF staining and statistical analysis in HepG2 cells. Scale bar: 50 μm. (D) HepG2 cells were treated with control DMEM or 300 μmol/L palmitate and incubated with 100 nmol/L Irisin for 24 h. LC3 protein expression was analyzed by Western blotting in the presence or absence of 50 μmol/L CQ (an inhibitor of autophagosome degradation, CQ) in HepG2 cells, and the corresponding statistical analysis was performed. (E1 and E2) LC3 expression in HepG2 cells was analyzed by immunofluorescence staining in the presence or absence of 50 μmol/L CQ, and the corresponding statistical analysis was performed. Scale bar: 50 μm. (F1 and F2) Fluorescence images reveal the colocalization of LC3 (green) and LAMP1 (red) in HepG2 cells. The Pearson correlation coefficient of LC3 and LAMP1 colocalization was obtained from 50 cells from three independent experiments. Scale bars: 10 μm. The data are presented as the mean ± SD. The values are from three independent experiments. $^{*}P$ <0.05, $^{**}P$ <0.01 *vs.* the control group, $^{\dagger}P$ <0.05 *vs.* the palmitate-treated group. CQ: Chloroquine; DMEM: Dulbecco's modified Eagle medium; GAPDH: Glyceraldehyde-3-phosphate dehydrogenase; LAMP1: Lysosome-associated protein 1; LC3: Light chain 3; nM: nmol/L; μM: μmol/L; PA: Palmitate; SD: Standard deviation.

a lysosomal protease crucial for protein degradation, was assessed.[37,38] Initially, cathepsin B protein levels were 40.8% lower in the HFD group (t = 11.7, P <0.05) than in the NCD group, according to the Western blotting analysis. Notably, treatment with Irisin led to a significant 1.3-fold increase (t = 3.9, P <0.05) in cathepsin B levels [Figure 4A]. Immunofluorescence analysis revealed that cathepsin B expression levels in the livers of the mice in the Irisin-treated group were significantly greater (t = 3.3, P <0.05) than that in the livers of the HFD group [Figure 4B]. These results were corroborated in HepG2 cells exposed to palmitate, where cathepsin B levels were 45.6% lower than those in the control group. However, this reduction was reversed with a 1.5-fold increase (t = 6.2, P <0.05) noted after Irisin treatment [Figure 4C]. Immunofluorescence analysis

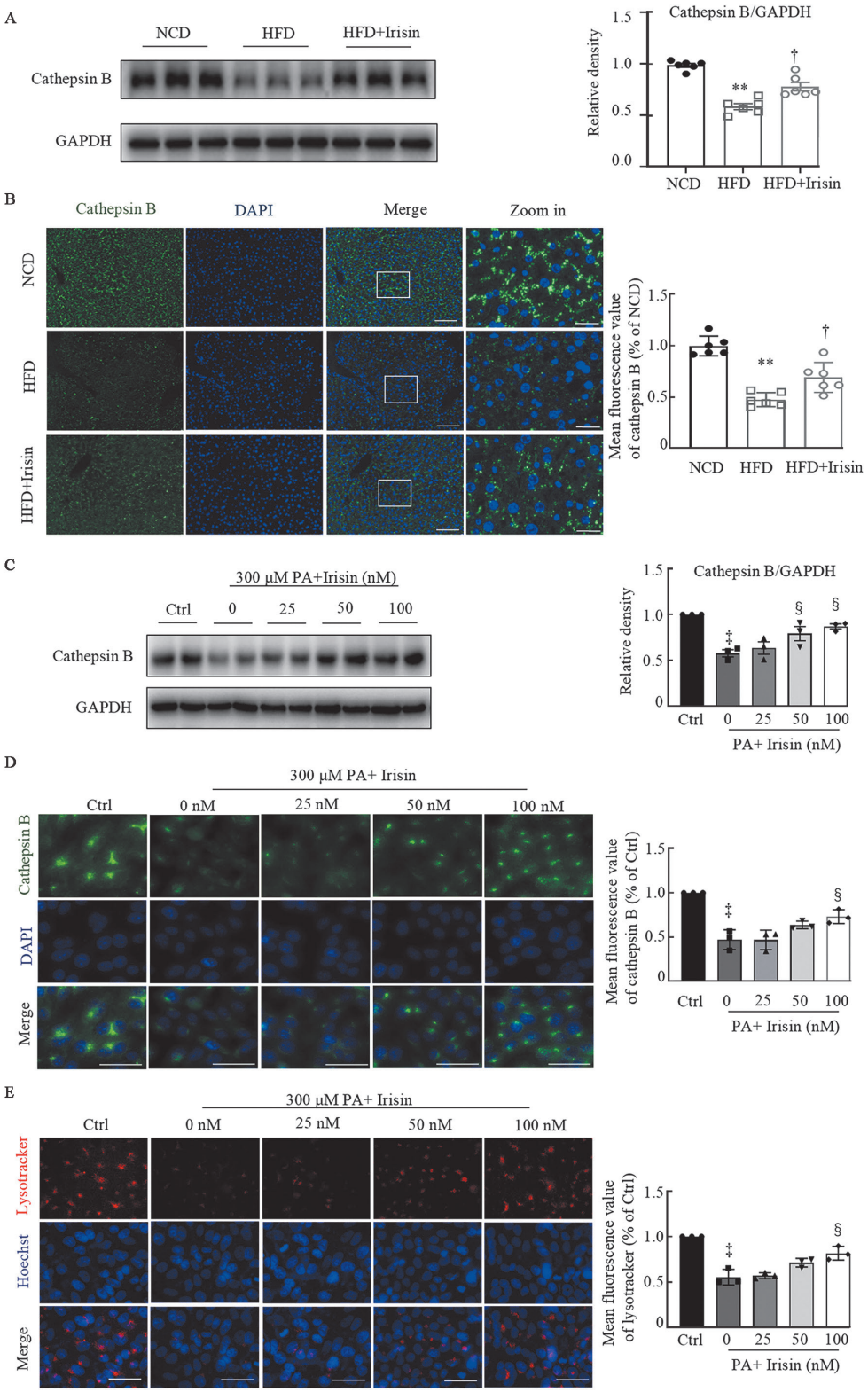

Figure 4: Irisin reduces hepatic lipid accumulation associated with improved lysosomal function in hepatocytes. (A) Cathepsin B expression levels in the livers of the mice in the normal diet, HFD, and Irisin groups at 16 weeks were analyzed by Western blotting and statistical analysis. (B) Cathepsin B expression levels in the livers of the mice in the normal diet, HFD, and Irisin groups at 16 weeks were analyzed by immunofluorescence staining and statistical analysis. The data are displayed as the mean ± SD and $n = 6$ for each of the three groups. The scale bar is 100 μm in the low-resolution image and 25 μm in the high-resolution image. (C) HepG2 cells were treated with control DMEM or 300 μmol/L palmitate and incubated with different doses of Irisin (0–100 nmol/L) for 24 h. Cathepsin B expression levels were analyzed by Western blotting and statistical analysis in HepG2 cells. (D) Cathepsin B expression levels are analyzed by immunofluorescence staining and statistical analysis in HepG2 cells. Scale bar: 50 μm. (E) LysoTracker levels were analyzed by immunofluorescence staining and statistical analysis in HepG2 cells. Scale bar: 50 μm. The data are displayed as the mean ± SD. The values are from three independent experiments. $^{*}P < 0.05$, $^{**}P < 0.01$ *vs.* NCD, $^{\dagger}P < 0.05$ *vs.* HFD, $^{\ddagger}P < 0.05$ *vs.* the untreated control group, $^{\S}P < 0.05$ *vs.* the palmitate-treated group. Ctrl: Control; CQ: Chloroquine; DAPI: 4′,6-iamidino-2-phenylindole dihydrochloride; GAPDH: Glyceraldehyde-3-phosphate dehydrogenase; HFD: High-fat diet; LAMP1: Lysosome-associated protein 1; LC3: Light chain 3; nM: nmol/L; μM: μmol/L; NCD: Normal chow diet; PA: Palmitate; SD: Standard deviation.

of cathepsin B in HepG2 cells further supported these findings [Figure 4D].

To gain further insight into lysosomal function, we used LysoTracker (a fluorescent dye for labeling acidic organelles, including lysosomes) to assess lysosomal acidity in HepG2 cells. Our results demonstrated that palmitic acid treatment reduced the fluorescence intensity of LysoTracker Red staining. In addition, as the Irisin concentration increased, the fluorescence intensity increased ($t = 3.9$, $P < 0.05$) [Figure 4E]. These findings suggest that irisin mitigates palmitic acid-induced alterations in lysosomal acidity. Collectively, our findings suggest that irisin enhances autophagic degradation through improved lysosomal function.

Irisin promotes autophagy partially by restoring the SIRT3/AMPK signaling pathway

In the liver, SIRT3 protein expression ($t = 13.1$, $P < 0.05$) and AMPK phosphorylation ($t = 8.2$, $P < 0.05$) were notably reduced by 33% and 43%, respectively, in the HFD-fed mice compared with the NCD-fed mice. However, treatment with Irisin significantly increased these levels by 1.2-fold ($t = 3.3$, $P < 0.05$) and 1.4-fold ($t = 3.2$, $P < 0.05$), respectively [Figure 5A]. Compared with that in the NCD group, mTOR phosphorylation levels were 2.2-fold greater ($t = 7.1$, $P < 0.05$) in the HFD group, but it was reduced by 32.1% following Irisin treatment ($t = 3.0$, $P < 0.05$). TFEB, which is present in the cytoplasm and nucleus, plays a critical role in lysosomal biogenesis by orchestrating the expression of lysosome-related genes.[39] Immunofluorescence staining of TFEB in the HFD group revealed that its translocation from the cytoplasm to the nucleus was inhibited ($t = 11.0$, $P < 0.05$), whereas its effect was partially improved ($t = 5.3$, $P < 0.05$) in the livers of Irisin-treated mice [Figure 5A]. These trends were consistent with the *in vitro* data. Palmitate inhibited SIRT3 protein expression ($t = 3.2$, $P < 0.05$) and AMPK phosphorylation ($t = 6.7$, $P < 0.05$), promoted mTOR phosphorylation ($t = 5.3$, $P < 0.05$), and inhibited the translocation of TFEB from the cytoplasm to the nucleus in HepG2 cells. These changes were partially reversed after treatment with Irisin ($t = 2.9$, $P < 0.05$) [Figure 5B].

To investigate whether Irisin enhances autophagic activity by modulating the SIRT3/AMPK pathway to reduce hepatic lipid accumulation, we used plasmids to overexpress SIRT3 and siRNAs to inhibit SIRT3 expression. Our results indicated that AMPK phosphorylation was increased ($t = 3.9$, $P < 0.05$) and that mTOR phosphorylation was further inhibited ($t = 8.4$, $P < 0.05$) in HepG2 cells treated with PA after SIRT3 overexpression compared with those in the PA treatment group. Moreover, when HepG2 cells were cotreated with PA and Irisin following SIRT3 overexpression, AMPK phosphorylation ($t = 3.9$, $P < 0.05$) was further promoted, and mTOR phosphorylation was further inhibited ($t = 5.9$, $P < 0.05$) compared with that in the PA and Irisin treatment groups. The increase in cathepsin B ($t = 4.0$, $P < 0.05$) expression and decrease in LC3 ($t = 6.8$, $P < 0.05$) and p62 expression ($t = 7.8$, $P < 0.05$) were associated with these changes [Figure 6A].

Conversely, when siRNA was used to knock down *SIRT3*, AMPK phosphorylation ($t = 11.0$, $P < 0.05$) and cathepsin B expression ($t = 5.7$, $P < 0.05$) were inhibited, and mTOR phosphorylation was promoted ($t = 4.8$, $P < 0.05$) in HepG2 cells cotreated with PA and Irisin, compared with those in the PA and Irisin treatment groups. Moreover, LC3 ($t = 3.9$, $P < 0.05$) and p62 ($t = 2.8$, $P < 0.05$) accumulation was observed in the PA and Irisin treatment groups in the context of *SIRT3* knockdown [Figure 6B]. ORO staining revealed that the number of lipid droplets in the Irisin treatment group was lower than that in the palmitate group. However, this improvement in lipid droplets was less pronounced ($t = 3.3$, $P < 0.05$) in the SIRT3 overexpression group, whereas the number of lipid droplets was greater ($t = 3.9$, $P < 0.05$) in the SIRT3 knockout group [Figure 6C, D]. These findings suggest that Irisin mitigates hepatic steatosis by modulating the SIRT3/AMPK signaling pathway [Figure 6E].

Discussion

This study demonstrated that administration of an irisin fusion protein weekly twice has a significant therapeutic effect on hepatic steatosis in HFD-induced MASLD. Irisin alleviates the accumulation of autophagosomes in hepatocytes induced by an HFD or palmitic acid by promoting the generation of lysosomes and enhancing the degradation of autolysosomes, thereby increasing autophagic flux and alleviating hepatic steatosis. The underlying mechanism is partially dependent on the SIRT3/AMPK signaling pathway.

Studies addressing irisin and lipid metabolism are ongoing. Recent studies have demonstrated that irisin improves lipid redistribution and reduces insulin resistance.[40] Our study provides compelling evidence for the therapeutic potential of irisin in the context of MASLD. By administering Irisin to HFD-induced MASLD model mice, we observed significant benefits in mitigating hepatic steatosis. We observed that Irisin visually reduced liver weight and lipid deposition in liver tissue in mice fed with HFD. The reductions in TG and TC levels in the serum and liver homogenate and the improvement in insulin resistance following Irisin administration underscore the importance of irisin in regulating lipid metabolism. In addition, Irisin also reduced ALT and AST levels in the serum of mice fed with HFD, confirming the important role of irisin in reducing liver damage. Notably, the effect of irisin on reducing hepatic lipid deposition appears to be more pronounced than its impact on body weight, underscoring its direct role in liver lipid metabolism.

Autophagy plays a pivotal role in liver lipid metabolism.[41] Impaired autophagy is associated with hepatic lipid accumulation and the development of steatosis.[42] Some studies have shown that autophagy-induced liver cell damage is associated with the onset and development of NAFLD. However, it should be noted that in the field of NAFLD research, there are differences in the phenomenon of liver autophagy.[43] Some studies have shown that LC3 protein expression is reduced and that p62 protein expression is increased under high fatty acid loading.[44] In our study, we observed the accumulation of the autophagosome

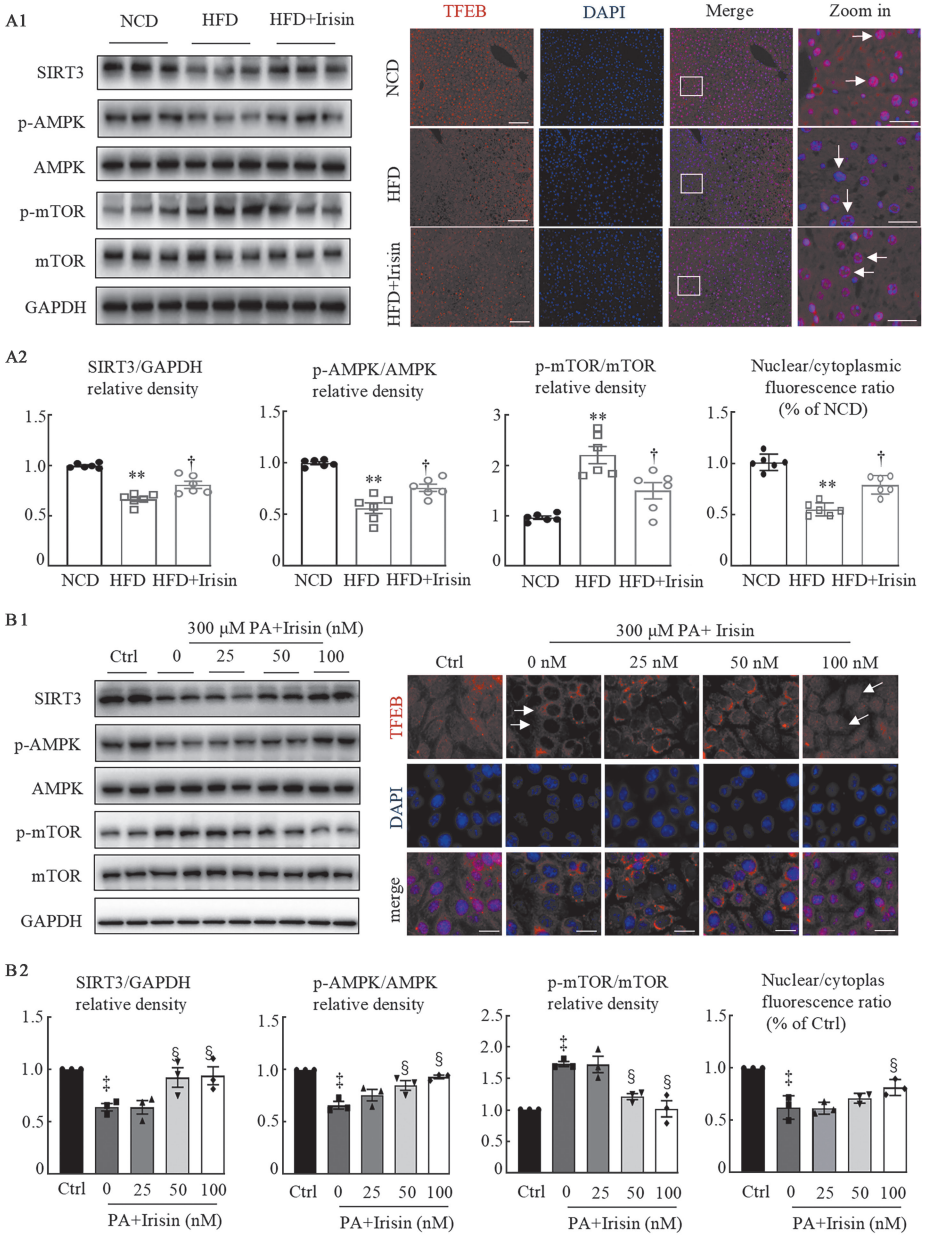

Figure 5: Irisin promotes autophagy partly by restoring the SIRT3/AMPK signaling pathway in hepatocytes. (A1) SIRT3, AMPK, and mTOR expression levels were analyzed via Western blotting, and the nuclear translocation of TFEB in the livers of the normal diet, HFD, and Irisin groups at 16 weeks was analyzed via immunofluorescence staining. (A2) Statistical analysis of SIRT3, AMPK, and mTOR expression levels and the nuclear translocation of TFEB. $n = 6$ for each of the three groups. The scale bar represents 100 μm in the low-resolution image and 25 μm in the high-resolution image. (B1) HepG2 cells were treated with control DMEM or 300 μmol/L palmitate or Irisin in the presence of various concentrations (0, 25, 50, 100 nmol/L) for 24 h. SIRT3, AMPK, and mTOR expression levels were analyzed via Western blotting, and the nuclear translocation of TFEB in HepG2 cells was analyzed via immunofluorescence staining. (B2) Statistical analysis of SIRT3, AMPK, and mTOR expression levels and the nuclear translocation of TFEB in HepG2 cells. The arrows represent the trans-location of the transcription factor TFEB in the cytoplasm and nucleus. Scale bar: 25 μm. The values are obtained from three independent experiments. The data are displayed as the mean ± SD. The bands corresponding to GAPDH in Figure 2: A, Figure 4: A, and Figure 5: A are the same images. $^{*}P < 0.05$ *vs.* NCD, $^{\dagger}P < 0.05$ *vs.* HFD. $^{\ddagger}P < 0.05$ *vs.* the untreated control group, $^{\S}P < 0.05$ *vs.* the palmitate-treated group. AMPK: AMP-activated protein kinase; Ctrl: Control; CQ: Chloroquine; GAPDH: Glyceraldehyde-3-phosphate dehydrogenase; HFD: High-fat diet; LAMP1: Lysosome-associated protein 1; LC3: Light chain 3; nM: nmol/L; μM: μmol/L; NCD: Normal chow diet; PA: Palmitate; SD: Standard deviation; SIRT3: Sirtuin 3; TFEB: Transcription factor EB.

markers LC3 and p62 in hepatocytes from MASLD mice and palmitic acid-treated HepG2 cells, indicating impaired autophagic flux due to reduced cargo degradation. This impairment was also evident in hepatocytes from MASLD patients, with the degree of accumulation correlating with disease severity.[45] Animal age, HFD conditions, feeding time, hepatocyte types, and fatty acids may also cause differences in autophagy.[46–48] We believe that time is also an essential factor in the differential manifestation of impaired autophagic flux when tissue cells respond to high lipid loads. Some studies have shown that the synthesis of autophagosomes increases in the early stage, but the degradation rate of autophagosomes is lower than their synthesis rate in HepG2 cells exposed to palmitate. Subsequently, the synthesis ability of autophagosomes gradually decreases to the basic state, and degradation disorders are the main manifestations. Ultimately, both the synthesis and degradation of autophagosomes are

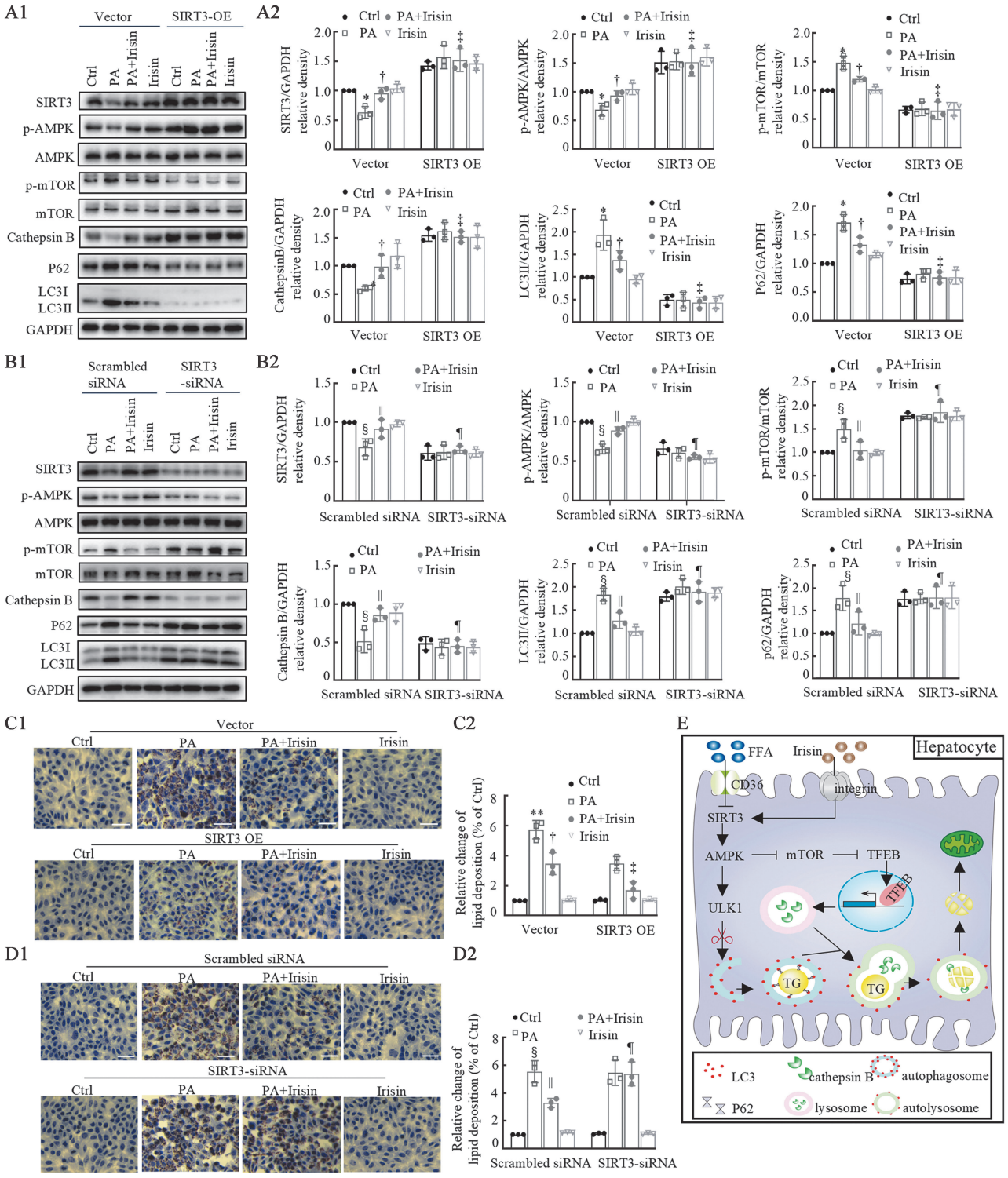

Figure 6: Changes in cell signaling pathways and lipid deposition in HepG2 cells caused by *SIRT3* overexpression or knockdown. (A1 and A2) Plasmids (0.5 μg) were transfected into the cells. After 24 h, the HepG2 cells were treated with control DMEM or 300 μmol/L palmitate and incubated with 100 nmol/L Irisin for 24 h. SIRT3, AMPK, mTOR, LC3, p62, and cathepsin B expression levels were analyzed via Western blotting and statistical analysis after the overexpression of SIRT3 in the HepG2 cells, which were then cotreated with different concentrations of Irisin and palmitate for 24 h. (B1 and B2) The cells were transfected with 50 nmol/L SIRT3-siRNA. After 24 h, the cells were treated with 300 μmol/L palmitic acid and 100 nmol/L Irisin (same time as before). SIRT3, AMPK, mTOR, LC3, p62, and cathepsin B expression levels in HepG2 cells after *SIRT3* knockdown and cotreatment with different concentrations of irisin and palmitate for 24 h were analyzed by Western blotting and statistical analysis. (C1 and C2) Representative images of ORO staining and statistical analysis in HepG2 cells after overexpression of SIRT3 and cotreatment with different concentrations of irisin and palmitate for 24 h. Scale bar: 50 μm. (D1 and D2) Representative image of ORO staining and statistical analysis of HepG2 cells after *SIRT3* knockdown and cotreatment with different concentrations of Irisin and palmitate for 24 h. Scale bar: 50 μm. (E) Irisin alleviates hepatic steatosis via the activation of the SIRT3/AMPK signaling pathway. The values are from three independent experiments. The data are displayed as the mean ± SD. $^{*}P$ <0.05 *vs.* the untreated control group with vector, $^{\dagger}P$ <0.05 *vs.* the palmitate-treated group with vector, $^{\ddagger}P$ <0.05 *vs.* the palmitate + Irisin-treated group with vector, $^{\S}P$ <0.05 *vs.* the untreated control group with scrambled siRNA, $^{\|}P$ <0.05 *vs.* the palmitate-treated group with scrambled siRNA, $^{\P}P$ <0.05 *vs.* the palmitate + Irisin-treated group with scrambled siRNA. AMPK: AMP-activated protein kinase; Ctrl: Control; GAPDH: Glyceraldehyde-3-phosphate dehydrogenase; HFD: High-fat diet; LC3: Light chain 3; mTOR: Mammalian target of rapamycin; ORO: Oil red O; SD: Standard deviation; SIRT3: Sirtuin 3.

reduced.[49] Therefore, the use of autophagy inhibitors provides a more dynamic understanding of the role of autophagy in reducing intracellular fat accumulation. To further substantiate the enhancement of autophagic flux in hepatocytes, we examined the effects of the autophagic degradation inhibitor CQ and assessed autolysosomes using confocal laser scanning microscopy. Our findings support the conclusion that irisin enhances autophagy by promoting the degradation of autophagosomes and the generation of autolysosomes.

Our study suggested that the effect of irisin may not depend on the initiation phase of autophagy, as evidenced by the lack of substantial changes in ULK1 phosphorylation, highlighting the role of irisin in the degradation phase of autophagy. Given that lysosomes play a pivotal role in autophagic degradation, we also examined the effect of irisin on lysosomal function. The results revealed the potential of irisin to improve lysosomal activity, as evidenced by the restoration of lysosomal protease cathepsin B levels and the maintenance of lysosomal acidity. Ultimately, Irisin promotes autophagy by enhancing the regeneration and activity of lysosomes. This leads to a substantial reduction in undegraded autophagy substrates, including p62 aggregates and lipid droplets, resulting in a marked amelioration of hepatic steatosis. These findings provide further insights into its therapeutic potential for MASLD.

The SIRT3/AMPK signaling pathway, which regulates autophagy, has emerged as a major factor in the effects of irisin.[50–52] A recent study revealed that irisin promotes osteogenesis and enhances longevity by regulating sirtuins and autophagy.[53,54] TFEB is a master regulator of autophagy and lysosomal function. TFEB increases autophagic flux by promoting the biogenesis of lysosomes and autophagosomes and fusing with lysosomes to efficiently degrade complex molecules.[55–57] The continuous shuttling of TFEB between the cytosol and the nucleus is regulated by mTOR-dependent phosphorylation.[58] Our findings suggest that Irisin administration restored SIRT3 expression, increased AMPK phosphorylation, inhibited mTOR activity, and promoted TFEB translocation from the cytoplasm to the nucleus, promoting lysosomal function. Plasmid-based SIRT3 overexpression in HepG2 cells increased autophagy and reduced lipid accumulation, supporting the role of SIRT3 as an upstream autophagy regulatory protein. Conversely, *SIRT3* knockdown attenuated the protective effects of Irisin. These results emphasize that irisin promotes autophagy through the SIRT3/AMPK signaling pathway to alleviate hepatic steatosis.

In conclusion, our study reveals that irisin is a promising therapeutic agent for MASLD by restoring the SIRT3/AMPK pathway, promoting TFEB translocation to the nucleus, thereby enhancing lysosomal function and further promoting autophagy. These findings provide more robust support that autophagy may represent a promising therapeutic target for MASLD. The direct role of irisin in hepatic lipid metabolism, independent of body weight, highlights its potential for the management of hepatic steatosis, which may represent one of the mechanisms by which exercise reduces hepatic lipids but not weight loss. Although our study has yielded valuable insights into the therapeutic potential of irisin for MASLD, exciting avenues for further research remain. Irisin not only has a significant lipid-lowering effect on fatty liver, but also reduces body fat and circulating lipids. Whether it can affect the lean mass of the body and its impact on muscles will be further studied. Notably, sex differences are undeniable factors in the study of MASLD, and future research needs to fully consider sex factors in animal models and clinical trials to ensure that the efficacy and safety evaluation of drugs truly reflect the situation in different sexes.[59–61] Future investigations should aim to confirm the precise liver receptors for irisin and explore specific receptors associated with lipophagy. These areas of study increase our understanding of the mechanisms of action of irisin and may reveal novel therapeutic strategies for liver-related disorders.

Funding

This work was partially supported by grants from the National Natural Science Foundation of China (Nos. 81570518, 82370814, and 81630020) and the Ministry of Science and Technology (No. 2017ZX09303001).

Conflicts of interest

None.

References

1. Rinella ME, Lazarus JV, Ratziu V, Francque SM, Sanyal AJ, Kanwal F, *et al*. A multisociety Delphi consensus statement on new fatty liver disease nomenclature. J Hepatol 2023;79:1542–1556. doi: 10.1016/j.jhep.2023.06.003.
2. Targher G, Byrne CD, Tilg H. MASLD: A systemic metabolic disorder with cardiovascular and malignant complications. Gut 2024;73:691–702. doi: 10.1136/gutjnl-2023-330595.
3. Hou M, Gu Q, Cui J, Dou Y, Huang X, Li J, *et al*. Proportion and clinical characteristics of metabolic-associated fatty liver disease and associated liver fibrosis in an urban Chinese population. Chin Med J 2024; Epub ahead of print. doi: 10.1097/CM9.0000000000003141.
4. Thyfault JP, Bergouignan A. Exercise and metabolic health: Beyond skeletal muscle. Diabetologia 2020;63:1464–1474. doi: 10.1007/s00125-020-05177-6.
5. Vilar-Gomez E, Martinez-Perez Y, Calzadilla-Bertot L, Torres-Gonzalez A, Gra-Oramas B, Gonzalez-Fabian L, *et al*. Weight loss through lifestyle modification significantly reduces features of nonalcoholic steatohepatitis. Gastroenterology 2015;149: 367–378.e5; quiz e14–5. doi: 10.1053/j.gastro.2015.04.005.
6. Cuthbertson DJ, Keating SE, Pugh CJA, Owen PJ, Kemp GJ, Umpleby M, *et al*. Exercise improves surrogate measures of liver histological response in metabolic dysfunction-associated steatotic liver disease. Liver Int 2024;44:2368–2381. doi: 10.1111/liv.15947.
7. Keating SE, Hackett DA, Parker HM, O'Connor HT, Gerofi JA, Sainsbury A, *et al*. Effect of aerobic exercise training dose on liver fat and visceral adiposity. J Hepatol 2015;63:174–182. doi: 10.1016/j.jhep.2015.02.022.
8. Sabag A, Barr L, Armour M, Armstrong A, Baker CJ, Twigg SM, *et al*. The effect of high-intensity interval training vs moderate-intensity continuous training on liver fat: A systematic review and meta-analysis. J Clin Endocrinol Metab 2022;107:862–881. doi: 10.1210/clinem/dgab795.
9. Keating SE, Sabag A, Hallsworth K, Hickman IJ, Macdonald GA, Stine JG, *et al*. Exercise in the management of metabolic-associated fatty liver disease (MAFLD) in adults: A position statement from exercise and sport science Australia. Sports Med 2023;53:2347–2371. doi: 10.1007/s40279-023-01918-w.

10. Zhang H, Wu X, Liang J, Kirberger M, Chen N. Irisin, an exercise-induced bioactive peptide beneficial for health promotion during aging process. Ageing Res Rev 2022;80:101680. doi: 10.1016/j.arr.2022.101680.
11. Maak S, Norheim F, Drevon CA, Erickson HP. Progress and challenges in the biology of FNDC5 and irisin. Endocr Rev 2021;42:436–456. doi: 10.1210/endrev/bnab003.
12. Guo M, Yao J, Li J, Zhang J, Wang D, Zuo H, *et al*. Irisin ameliorates age-associated sarcopenia and metabolic dysfunction. J Cachexia Sarcopenia Muscle 2023;14:391–405. doi: 10.1002/jcsm.13141.
13. Zhang HJ, Zhang XF, Ma ZM, Pan LL, Chen Z, Han HW, *et al*. Irisin is inversely associated with intrahepatic triglyceride contents in obese adults. J Hepatol 2013;59:557–562. doi: 10.1016/j.jhep.2013.04.030.
14. Kosmalski M, Drzewoski J, Szymczak-Pajor I, Zieleniak A, Mikołajczyk-Solińska M, Kasznicki J, *et al*. Irisin is related to non-alcoholic fatty liver disease (NAFLD). Biomedicines 2022;10:2253. doi: 10.3390/biomedicines10092253.
15. Qiu S, Wang Q, Cai X, Sun Z, Wu T. Circulating irisin in nonalcoholic fatty liver disease: An updated meta-analysis. Endokrynol Pol 2023;74:47–54. doi: 10.5603/EP.a2022.0067.
16. Xin C, Liu J, Zhang J, Zhu D, Wang H, Xiong L, *et al*. Irisin improves fatty acid oxidation and glucose utilization in type 2 diabetes by regulating the AMPK signaling pathway. Int J Obes (Lond) 2016;40:443–451. doi: 10.1038/ijo.2015.199.
17. Yano N, Zhang L, Wei D, Dubielecka PM, Wei L, Zhuang S, *et al*. Irisin counteracts high glucose and fatty acid-induced cytotoxicity by preserving the AMPK-insulin receptor signaling axis in C2C12 myoblasts. Am J Physiol Endocrinol Metab 2020;318:E791–E805. doi: 10.1152/ajpendo.00219.2019.
18. Tang H, Yu R, Liu S, Huwatibieke B, Li Z, Zhang W. Irisin inhibits hepatic cholesterol synthesis via AMPK-SREBP2 signaling. EBioMedicine 2016;6:139–148. doi: 10.1016/j.ebiom.2016.02.041.
19. Li H, Shen J, Wu T, Kuang J, Liu Q, Cheng S, *et al*. Irisin is controlled by farnesoid X receptor and regulates cholesterol homeostasis. Front Pharmacol 2019;10:548. doi: 10.3389/fphar.2019.00548.
20. Xiong XQ, Chen D, Sun HJ, Ding L, Wang JJ, Chen Q, *et al*. FNDC5 overexpression and irisin ameliorate glucose/lipid metabolic derangements and enhance lipolysis in obesity. Biochim Biophys Acta 2015;1852:1867–1875. doi: 10.1016/j.bbadis.2015.06.017.
21. Zhu W, Sahar NE, Javaid HMA, Pak ES, Liang G, Wang Y, *et al*. Exercise-induced irisin decreases inflammation and improves NAFLD by competitive binding with MD2. Cells 2021;10:3306. doi: 10.3390/cells10123306.
22. Kumar M, Hunag Y, Glinka Y, Prud'homme GJ, Wang Q. Gene therapy of diabetes using a novel GLP-1/IgG1-Fc fusion construct normalizes glucose levels in db/db mice. Gene Ther 2007;14:162–172. doi: 10.1038/sj.gt.3302836.
23. Soltani N, Kumar M, Glinka Y, Prud'homme GJ, Wang Q. *In vivo* expression of GLP-1/IgG-Fc fusion protein enhances beta-cell mass and protects against streptozotocin-induced diabetes. Gene Ther 2007;14:981–988. doi: 10.1038/sj.gt.3302944.
24. Kazeminasab F, Sadeghi E, Afshari-Safavi A. Comparative impact of various exercises on circulating irisin in healthy subjects: A systematic review and network meta-analysis. Oxid Med Cell Longev 2022;2022:8235809. doi: 10.1155/2022/8235809.
25. Filali-Mouncef Y, Hunter C, Roccio F, Zagkou S, Dupont N, Primard C, *et al*. The ménage à trois of autophagy, lipid droplets and liver disease. Autophagy 2022;18:50–72. doi: 10.1080/15548627.2021.1895658.
26. Shin DW. Lipophagy: Molecular mechanisms and implications in metabolic disorders. Mol Cells 2020;43:686–693. doi: 10.14348/molcells.2020.0046.
27. Han YH, He XM, Jin MH, Sun HN, Kwon T. Lipophagy: A potential therapeutic target for nonalcoholic and alcoholic fatty liver disease. Biochem Biophys Res Commun 2023;672:36–44. doi: 10.1016/j.bbrc.2023.06.030.
28. An L, Wirth U, Koch D, Schirren M, Drefs M, Koliogiannis D, *et al*. Metabolic role of autophagy in the pathogenesis and development of NAFLD. Metabolites 2023;13:101. doi: 10.3390/metabo13010101.
29. Dashti Z, Yousefi Z, Kiani P, Taghizadeh M, Maleki MH, Borji M, *et al*. Autophagy and the unfolded protein response shape the non-alcoholic fatty liver landscape: Decoding the labyrinth. Metabolism 2024;154:155811. doi: 10.1016/j.metabol.2024.155811.
30. Liu TY, Xiong XQ, Ren XS, Zhao MX, Shi CX, Wang JJ, *et al*. FNDC5 alleviates hepatosteatosis by restoring AMPK/mTOR-mediated autophagy, fatty acid oxidation, and lipogenesis in mice. Diabetes 2016;65:3262–3275. doi: 10.2337/db16-0356.
31. Mauthe M, Orhon I, Rocchi C, Zhou X, Luhr M, Hijlkema KJ, *et al*. Chloroquine inhibits autophagic flux by decreasing autophagosome-lysosome fusion. Autophagy 2018;14:1435–1455. doi: 10.1080/15548627.2018.1474314.
32. Klionsky DJ, Abdel-Aziz AK, Abdelfatah S, Abdellatif M, Abdoli A, Abel S, *et al*. Guidelines for the use and interpretation of assays for monitoring autophagy (4th edition)[1]. Autophagy 2021;17:1–382. doi: 10.1080/15548627.2020.1797280.
33. Lonardo A, Ballestri S, Mantovani A, Targher G, Bril F. Endpoints in NASH clinical trials: Are we blind in one eye? Metabolites 2024;14:40. doi: 10.3390/metabo14010040.
34. Tilg H, Byrne CD, Targher G. NASH drug treatment development: Challenges and lessons. Lancet Gastroenterol Hepatol 2023;8:943–954. doi: 10.1016/s2468-1253(23)00159-0.
35. Sankar DS, Kaeser-Pebernard S, Vionnet C, Favre S, de Oliveira Marchioro L, Pillet B, *et al*. The ULK1 effector BAG2 regulates autophagy initiation by modulating AMBRA1 localization. Cell Rep 2024;43:114689. doi: 10.1016/j.celrep.2024.114689.
36. Yang C, Wang X. Lysosome biogenesis: Regulation and functions. J Cell Biol 2021;220:e202102001. doi: 10.1083/jcb.202102001.
37. Man SM, Kanneganti TD. Regulation of lysosomal dynamics and autophagy by CTSB/cathepsin B. Autophagy 2016;12:2504–2505. doi: 10.1080/15548627.2016.1239679.
38. Zeng J, Acin-Perez R, Assali EA, Martin A, Brownstein AJ, Petcherski A, *et al*. Restoration of lysosomal acidification rescues autophagy and metabolic dysfunction in non-alcoholic fatty liver disease. Nat Commun 2023;14:2573. doi: 10.1038/s41467-023-38165-6.
39. Tan A, Prasad R, Lee C, Jho EH. Past, present, and future perspectives of transcription factor EB (TFEB): Mechanisms of regulation and association with disease. Cell Death Differ 2022;29:1433–1449. doi: 10.1038/s41418-022-01028-6.
40. Aladag T, Mogulkoc R, Baltaci AK. Irisin and energy metabolism and the role of irisin on metabolic syndrome. Mini Rev Med Chem 2023;23:1942–1958. doi: 10.2174/1389557523666230411105506.
41. Zhang S, Peng X, Yang S, Li X, Huang M, Wei S, *et al*. The regulation, function, and role of lipophagy, a form of selective autophagy, in metabolic disorders. Cell Death Dis 2022;13:132. doi: 10.1038/s41419-022-04593-3.
42. Velikova T, Gulinac M. Novel insights into autophagy in gastrointestinal pathologies, mechanisms in metabolic dysfunction-associated fatty liver disease and acute liver failure. World J Gastroenterol 2024;30:3273–3277. doi: 10.3748/wjg.v30.i27.3273.
43. Jin S, Li Y, Xia T, Liu Y, Zhang S, Hu H, *et al*. Mechanisms and therapeutic implications of selective autophagy in nonalcoholic fatty liver disease. J Adv Res 2024;S2090-1232:00041–9. doi: 10.1016/j.jare.2024.01.027.
44. Zhang T, Liu J, Shen S, Tong Q, Ma X, Lin L. SIRT3 promotes lipophagy and chaperon-mediated autophagy to protect hepatocytes against lipotoxicity. Cell Death Differ 2020;27:329–344. doi: 10.1038/s41418-019-0356-z.
45. González-Rodríguez A, Mayoral R, Agra N, Valdecantos MP, Pardo V, Miquilena-Colina ME, *et al*. Impaired autophagic flux is associated with increased endoplasmic reticulum stress during the development of NAFLD. Cell Death Dis 2014;5:e1179. doi: 10.1038/cddis.2014.162.
46. Liu X, Li X, Su S, Yuan Y, Liu W, Zhu M, *et al*. Oleic acid improves hepatic lipotoxicity injury by alleviating autophagy dysfunction. Exp Cell Res 2023;429:113655. doi: 10.1016/j.yexcr.2023.113655.
47. Zhao J, Hu Y, Peng J. Targeting programmed cell death in metabolic dysfunction-associated fatty liver disease (MAFLD): A promising new therapy. Cell Mol Biol Lett 2021;26:17. doi: 10.1186/s11658-021-00254-z.
48. Ren Q, Sun Q, Fu J. Dysfunction of autophagy in high-fat diet-induced non-alcoholic fatty liver disease. Autophagy 2024;20:221–241. doi: 10.1080/15548627.2023.2254191.
49. Ding H, Ge G, Tseng Y, Ma Y, Zhang J, Liu J. Hepatic autophagy fluctuates during the development of non-alcoholic fatty liver disease. Ann Hepatol 2020;19:516–522. doi: 10.1016/j.aohep.2020.06.001.
50. Sun R, Kang X, Zhao Y, Wang Z, Wang R, Fu R, *et al*. Sirtuin 3-mediated deacetylation of acyl-CoA synthetase family member 3

by protocatechuic acid attenuates non-alcoholic fatty liver disease. Br J Pharmacol 2020;177:4166–4180. doi: 10.1111/bph.15159.
51. Sánchez B, Muñoz-Pinto MF, Cano M. Irisin enhances longevity by boosting SIRT1, AMPK, autophagy and telomerase. Expert Rev Mol Med 2022;25:e4. doi: 10.1017/erm.2022.41.
52. Hua X, Hou M, Deng L, Lv N, Xu Y, Zhu X, *et al*. Irisin-loaded electrospun core-shell nanofibers as calvarial periosteum accelerate vascularized bone regeneration by activating the mitochondrial SIRT3 pathway. Regen Biomater 2023;11:rbad096. doi: 10.1093/rb/rbad096.
53. Li G, Qin H, Zhou M, Zhang T, Zhang Y, Ding H, *et al*. Knockdown of SIRT3 perturbs protective effects of irisin against bone loss in diabetes and periodontitis. Free Radic Biol Med 2023;200:11–25. doi: 10.1016/j.freeradbiomed.2023.02.023.
54. Li G, Jian Z, Wang H, Xu L, Zhang T, Song J. Irisin promotes osteogenesis by modulating oxidative stress and mitophagy through SIRT3 signaling under diabetic conditions. Oxid Med Cell Longev 2022;2022:3319056. doi: 10.1155/2022/3319056.
55. Dwivedi R, Baindara P. Differential regulation of TFEB-induced autophagy during MTB infection and starvation. Microorganisms 2023;11:2944. doi: 10.3390/microorganisms11122944.
56. Shariq M, Khan MF, Raj R, Ahsan N, Kumar P. PRKAA2, MTOR, and TFEB in the regulation of lysosomal damage response and autophagy. J Mol Med (Berl) 2024;102:287–311. doi: 10.1007/s00109-023-02411-7.
57. Franco-Juárez B, Coronel-Cruz C, Hernández-Ochoa B, Gómez-Manzo S, Cárdenas-Rodríguez N, Arreguin-Espinosa R, *et al*. TFEB; beyond its role as an autophagy and lysosomes regulator. Cells 2022;11:3153. doi: 10.3390/cells11193153.
58. Cui Z, Napolitano G, de Araujo MEG, Esposito A, Monfregola J, Huber LA, *et al*. Structure of the lysosomal mTORC1-TFEB-Rag-Ragulator megacomplex. Nature 2023;614:572–579. doi: 10.1038/s41586-022-05652-7.
59. Lonardo A, Nascimbeni F, Ballestri S, Fairweather D, Win S, Than TA, *et al*. Sex differences in nonalcoholic fatty liver disease: State of the art and identification of research gaps. Hepatology 2019;70:1457–1469. doi: 10.1002/hep.30626.
60. Burra P, Zanetto A, Germani G. Sex bias in clinical trials in gastroenterology and hepatology. Nat Rev Gastroenterol Hepatol 2022;19:413–414. doi: 10.1038/s41575-022-00638-2.
61. Burra P, Bizzaro D, Gonta A, Shalaby S, Gambato M, Morelli MC, *et al*. Clinical impact of sexual dimorphism in non-alcoholic fatty liver disease (NAFLD) and non-alcoholic steatohepatitis (NASH). Liver Int 2021;41:1713–1733. doi: 10.1111/liv.14943.

How to cite this article: Zhao Y, Li J, Ma AR, Wang ZH, Ni YZ, Wu D, Zhou Y, Zhang N, Zhang L, Chang YS, Wang QH. Irisin alleviates hepatic steatosis by activating the autophagic SIRT3 pathway. Chin Med J 2026;139:443–456. doi: 10.1097/CM9.0000000000003427